IEEE Access
Multidisciplinary | Rapid Review | Open Access Journal

Received January 16, 2021, accepted January 19, 2021, date of publication January 22, 2021, date of current version January 29, 2021.

Digital Object Identifier 10.1109/ACCESS.2021.3053625

Investigation of Base High Doping Impact on the npn Solar Cell Microstructure Performance Using Physically Based Analytical Model

MARWA S. S. BASYONI[1,2], A. ZEKRY[3], (Member, IEEE), AND AHMED SHAKER[4]

[1]Department of Computer Engineering, Computer Science and Engineering College, University of Ha'il, Ha'il 81451, Saudi Arabia
[2]Department of Electrical Communication and Electronics Systems Engineering, Faculty of Engineering, Modern Science and Arts University (MSA), Cairo 12451, Egypt
[3]Department of Electronics and Communications, Faculty of Engineering, Ain Shams University, Cairo 11517, Egypt
[4]Department of Engineering Physics and Mathematics, Faculty of Engineering, Ain Shams University, Cairo 11517, Egypt

Corresponding author: Ahmed Shaker (ahmed.shaker@eng.asu.edu.eg)

This work was supported by the Deanship of Scientific Research at the University of Ha'il under Project RG-191279.

ABSTRACT Recently, there is a rapid trend to incorporate low cost solar cells in photovoltaic technology. In this regard, low-cost high-doped Silicon wafers are beneficial; however, the high doping effects encountered in these wafers render their practical use in fabrication. The npn solar cell microstructure has been found to avoid this issue by the proper design of vertical generation and lateral collection of the light generated carriers. We report on the impact of the p^+ base doping concentration, up to $2 \times 10^{19}cm^{-3}$, on the npn microstructure performance to find the most appropriate way for high efficiency. To optimize the structure, a series of design steps has been applied using our previously published analytical model. Before inspecting the high doped base effect, firstly, the n^+ emitter is optimized. Secondly, the impact of bulk recombination inside the p^+ base is introduced showing the range of optimum base width (W_p). Then, we investigate thoroughly the impact of base doping levels for different base widths to get the optimum W_p that satisfies maximum efficiency. The results show that for p^+ base doping concentration ranging from $5 \times 10^{17}cm^{-3}$ to $2 \times 10^{19}cm^{-3}$, the npn microstructure efficiency decreases from 15.9% to 9%, respectively. Although the efficiency is degraded considerably for higher doping levels, the structure still achieves a competitive efficiency at higher doping levels, for which its cost is greatly reduced, in comparison with thin film solar cells. Moreover, using higher doping permits lesser wafer area which could be beneficial for large area solar cells design.

INDEX TERMS Analytical modeling, high doping, high efficiency, low cost, P^+ base doping.

I. INTRODUCTION

Solar cell technology is one of the fastest developing fields nowadays. In the last few years, the single crystalline silicon solar cells were competed by the thin-film solar cells (TFSCs) due to the low cost of TFSCs and the rapid improvement in its efficiency [1]. However, TFSCs have some restrictions, such as their limited effectiveness in absorbing the long wavelengths of solar radiation spectrum due to the small thickness of its active layer [2]. Besides, most of TFSCs encounter toxic materials in their structures [3]. Those are some of the reasons behind that TFSCs need more researches and investigations to be commercially available.

The associate editor coordinating the review of this manuscript and approving it for publication was Wen-Sheng Zhao.

Meanwhile, solar cells fabricated from silicon are efficient, reliable and stable. The silicon-based solar cells still cover around 90% of the PV systems market. However, the high efficiency of planar solar cell cost is still high compared to TFSCs [4], [5]. Therefore, recent researches focus on fabricating silicon-based solar cells using cheap ways while achieving high efficiency [6]–[9]. One of the interesting ways to reduce the cell cost is by using a silicon nanorod. It has a heavily doped pn junction in the radial direction [10], [11]. However, the fabrication difficulties set a limit to the wide spread of this type of solar cells. Other efforts carried out by our research group are still in progress to achieve high efficiency low-cost solar cell structure, which satisfies the industry demand [12]–[16]. To achieve low cost solar cells, the substrate must be made of inexpensive materials which

generally suffer from defects. These defects are responsible of reducing the minority carrier diffusion length [17], [18] which, in turn, results in cell performance deterioration. To overcome this issue, the light generated carriers must be vertically generated and laterally collected. Thus, the low-quality and low-cost heavily doped silicon wafers could be used in solar cells, as previously demonstrated by TCAD simulation using process and device simulators [13]–[15].

Analytical models are vital in understanding the device behavior before trying fabrication process complication. Analytical models are used extensively in investigating new device architectures and optimization of device parameters to pursuit the best performance. It has been confirmed extensively that physically based analytical models are efficient means to explore solar cells behavior [10], [19], [20]. The dependence of solar cells characteristics on their various design parameters could be inspected analytically with no need for high TCAD simulation times or fabrication cost and difficulty. Further, analytical models provide a transparent solution, and the influence of the different parameters is easily and rapidly assessed. Besides, the performance limits of the device could be realized in a simple way and short times.

In [16], we developed a physically based analytical model which has shown a good accuracy and fast computational time compared to TCAD simulation. In this work, our aim is to use our previously published model to illustrate the impact of p^+ base doping variation on the npn solar cell microstructure performance. Thus, the most appropriate way for achieving high efficiency and low-cost silicon-based solar cells could be obtained. The npn microstructure analytical model [16] is used to optimize the structure performance thought a series of design steps.

In this paper, firstly, a quick view of the npn structure, used in this work, is presented in Section II along with the main design parameters. The analytical model [16] is reviewed in Section III. Next, the enhancement of the npn highly doped wafers based solar cell microstructure is studied in terms of the following steps. Firstly, in Section IV, the n^+ emitter optimization is carried out for its sidewall surface treatment then its doping concentration is optimized. Secondly, in Section V, the effect of bulk recombination inside the p^+ base (W_p) on the structure performance is inspected. In Section VI, the impact of p^+ doping variation, from 5×10^{17} cm^{-3}up to $2 \times 10^{19} cm^{-3}$, on the npn structure performance is illustrated. All simulations are carried out using our analytical model implemented in MATLAB environment [16]. Finally, a summary of the essential findings and conclusions of this work is drawn in Section VII.

II. MAIN npn MICROSTRUCTURE AND DESIGN PARAMETERS

Fig. 1 shows the basic structure of the npn solar cell under investigation. Fig. 1(a) demonstrates the structure three-dimensional view and clarifies the structure unit cell which is repeated along the whole wafer. The structure is based on

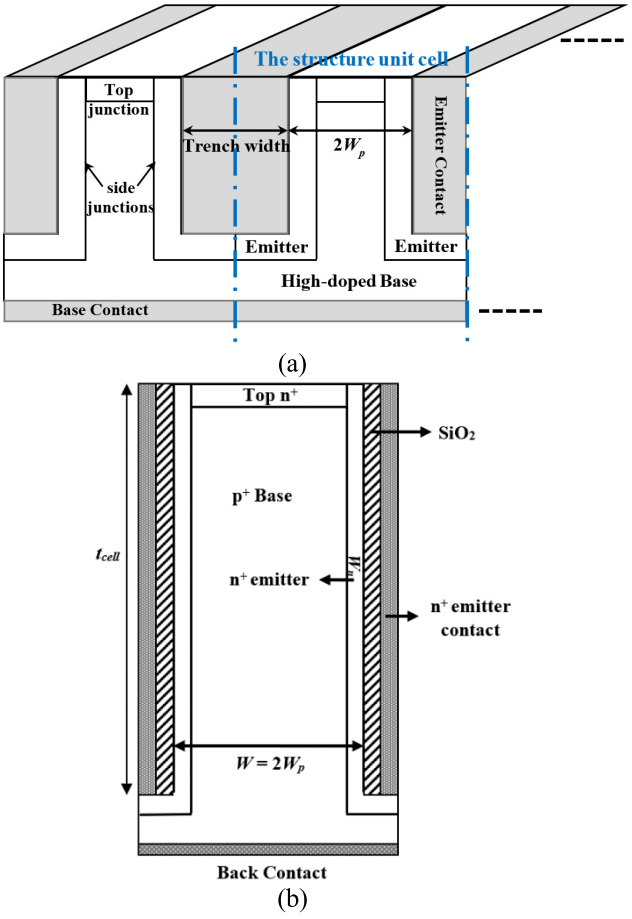

FIGURE 1. Basic npn microstructure (a) 3D view of adjacent cells and (b) detailed description of unit cell parameters where the side wall and top pn junctions and surface treatment with SiO_2 are illustrated.

using a heavily doped p-type wafer to form the p^+-base. For each unit cell, two pn junctions are formed. A vertical principal one, which is called the side wall pn junction, consists of n^+ region aside with the base. The main function of this junction is the lateral collection of the vertically produced carriers from the normal incident solar radiation. The other one, which is a secondary junction, is called the top pn junction which consists of an n^+ region over the base and it contributes to collecting a considerable portion of the input radiation which, in turn, results in increasing the efficiency.

The criterion of using high-doped wafers is stated as follows. As the purity of the silicon increases, it will be more expensive. Actually, solar-grade crystalline Si (c-Si) is expensive at \$20–30 per kg because of the various treatment methods required for purification [21]. Currently, the production cost of the Si wafers makes 40% of the solar panels overall cost [22]. To reduce the purification steps of the solar grade silicon and thereby significantly reduce the cost, one should make solar cells from heavily doped silicon wafers that do not need multiple zone-refining processes. In this regard, metallurgical grade c-Si wafers are inexpensive at \$1.75–2.30 per kg [21]; however, it is not used in conventional

planar solar cells due to its low efficiency resulting from the low diffusion length caused by high impurity densities. In our design, unlike planar cells, the npn microstructure provides the benefit of decoupling the processes of light absorption and carrier collection into vertical and lateral directions, respectively. This impact facilitates the use of short diffusion lengths which are encountered in high-doped wafers. So, our investigations on the yield of the heavily doped silicon can reduce the manufacturing cost. Further, our target is to produce solar cells having the highest possible doping and efficiency, i.e. maximum efficiency-to-cost ratio.

The proposed npn structure fabrication requires the same traditional process flow of conventional planar solar cell fabrication processes. The only additional step is to open the vertical notches by producing deep trenches to form vertical sidewall electrodes. This additional fabrication step could be achieved by a low-cost metal-assisted chemical etching method [23]. Then, the emitter metal could be evaporated, and the top metallic layer could be removed by commercial tapes, instead of the costly ion milling, which more reduces the fabrication cost [24].

The main parameters of the npn solar cell structure, shown in Fig. 1(b), are as follows. The width W is the cell base width which is equal to $2W_p$ where W_p is the width of the p-region part of the side wall pn junction while the width of the n^+ side wall is termed by W_n and the thickness of the cell is denoted by t_{cell}. The doping of the p-base, side wall n^+ and top n^+ regions are termed $N_{p+,base}$, $N_{n+,emitter}$ and $N_{n+,top}$, respectively. The n^+ top layer thickness is $t_{n+,top}$. The surface treatment is illustrated in Fig. 1(b), where SiO_2 (with a thickness t_{SiO2}) is used before deposition of the aluminum contact. This forms a polysilicon emitter-like contact in which current flows from the contact to the cell via tunneling. Also, this type of contacts reduces the surface recombination substantially as will be discussed herein.

The main design parameters of the solar cell microstructure are summarized in Table 1. The criteria of using such design parameters values were discussed in our previous work [15]. In [15], it was found by TCAD extensive simulations that it is more useful to make the top and side n^+ junctions having the same doping and thickness. This is also favorable from the fabrication point of view as, that way, the top and side junctions can be formed in a single diffusion process. Based on this cell modification, higher efficiencies, up to about 15%, could be obtained [15]. In the next section, we are going to present the main equations that constitute the core analytical model used in this work. The detailed modeling technique and derivations are found in [16].

III. MODEL METHODOLOGY

Our analytical model is based on the solution of the 1D drift diffusion model, in which the electron current density is given by,

$$J_n = q\mu_n E + qD_n \frac{\delta\, \Delta n}{\delta x} \tag{1}$$

TABLE 1. Main npn solar cell technological parameters.

Parameter	Value
W_p	8 µm
$t_{n+,top}$	0.1 µm
W_n	0.1 µm
t_{cell}	80 µm
$N_{p+,base}$	10^{18} cm^{-3}
$N_{n+,emitter}$	5×10^{19} cm^{-3}
$N_{n+,top}$	5×10^{19} cm^{-3}

where Δn is the excess electron concentration. All other physical parameters are defined in the Appendix. Further, at steady state conditions, the continuity equation could be formulated as,

$$\frac{1}{q}\frac{\delta J_n}{\delta x} - U + g_{ph}\,(y, \lambda) = 0 \tag{2}$$

where $U = \Delta n/\tau_n$ and g_{ph} are the recombination and photogeneration rates (given in cm^{-3}s^{-1}), respectively. The electron lifetime, τ_n, is the effective lifetime which comprises both the Shockley Read Hall and Auger recombination. As our base doping is high, Auger recombination is significant in this case and cannot be ignored.

Combining (2) and (1), one can write,

$$\frac{\delta^2\, \Delta n}{\delta x^2} - \frac{\Delta n}{L_n^2} + \tau_n\, g_{ph}\,(y, \lambda) = 0 \tag{3}$$

Similar expressions could be written for holes as in [16]. Also, all physical parameters related to holes are found in the Appendix. Next, we are going to get the excess carrier concentrations in both short circuit and dark conditions in to get the current density through the cell.

A. SHORT CIRCUIT CASE

Fig. 2 shows a representation of the excess electron and hole concentrations inside the base and emitter. Fig. 2(a) illustrates the excess electron concentration showing the boundary conditions at the center of the base and at the base-emitter depletion region edge. On the other hand, the excess hole concentration is drawn in Fig. 2(b). Also, the boundary conditions are illustrated at the emitter-base depletion region edge and the emitter-contact edge.

Applying the boundary conditions illustrated in Fig. 2(a), we can solve (3) to get $\Delta n(x)$ for the short circuit case,

$$\Delta n\,(x) = \frac{\tau_n g_{ph}\,(y, \lambda)\,[1 - \cosh\,(x/L_n)]}{\cosh\left(W_p/L_n\right)} \tag{4}$$

Then, we can get $J_n(x)$,

$$J_n = q g_{ph}\,(y, \lambda)\, L_n \tanh\left(\frac{W_p}{L_n}\right) \tag{5}$$

Regarding hole current density inside the n^+ region, the boundary conditions are found from Fig. 2(b). Applying these boundary conditions, we can find,

$$\Delta p\,(x) = A_p e^{-x/L_p} + B_p\, e^{x/L_p} + \tau_p\, g_{ph}\,(y, \lambda) \tag{6}$$

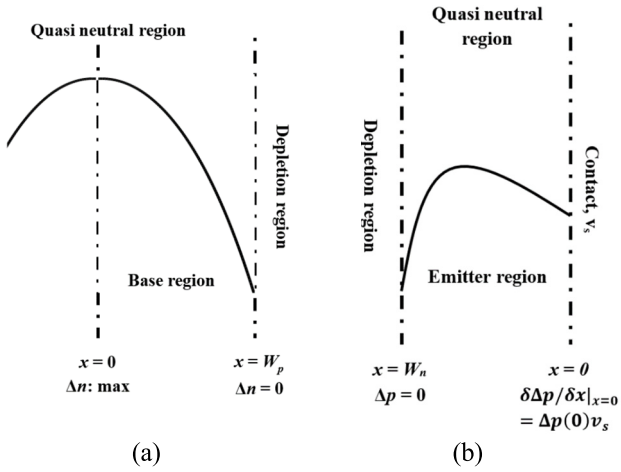

FIGURE 2. Excess concentration at short circuit condition (a) electrons inside base, (b) holes inside emitter. The boundary conditions for both excess electron and hole concentrations are illustrated.

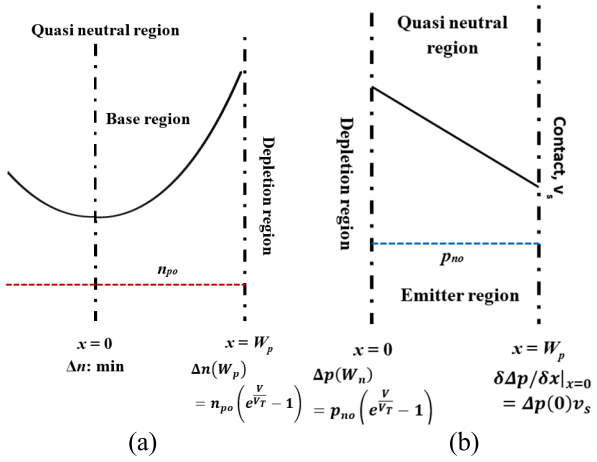

FIGURE 3. Excess concentrations at dark condition (a) electrons inside base, (b) holes inside emitter. The boundary conditions for both excess electron and hole concentrations are also illustrated.

where the constants A and B could be found in the Appendix (Equations A.1 and A.2). The hole/electron lifetime is taken as a function of doping concentration and is given by,

$$\tau_{p/n} = \frac{\tau_{po/no}}{1 + \left(N_{dop}/N_{ref}\right)^{\gamma}}$$

where $N_{ref} = 5\times10^{16}\ \mathrm{cm}^{-3}$, N_{dop} is the doping concentration in cm^{-3} and τ_{po} and τ_{no} are determined from measured samples of n+ emitters [25] and high doped p+ bases [26]. The constant γ is assumed to be 0.5 according to [27].

Now, the hole current density at short circuit is,

$$J_p = \frac{qD_p}{L_p}\left[A_p e^{\frac{-W_n}{L_p}} - B_p e^{\frac{W_n}{L_p}}\right] \tag{7}$$

Finally, the overall short circuit current density is the summation of J_n and J_p, equations (5) and (7), multiplied by two as we have two emitters,

$$J_{sc} = 2 \times \left(J_n + J_p\right) \tag{8}$$

B. DARK CASE

Regarding the dark condition, Fig. 3(a) represents the excess electron concentration showing the boundary conditions at the center of the base and at the base-emitter depletion region edge. Similarly, the excess hole concentration is represented in Fig. 3(b). Also, the boundary conditions are shown at the emitter-base depletion region edge and the emitter-contact edge.

In the dark case, there is no photo generation rate, thus $g_{ph} = 0$. In order to get the excess electron concentration in the base, in this case, we can formulate the boundary conditions as seen in Fig. 3(a). Where $n_{po} = n_{ie}^2/N_d$ and $n_{po} = n_{ie}^2/N_d$. ΔE_g is the band gap shift due to band gap narrowing resulting from high doping levels impact, k is Boltzmann's constant, and T is the absolute temperature. In our analysis, we used the BGN model by Slot boom [28].

Now, \ applying these boundary conditions, we can find that,

$$\Delta n\,(x) = \left[\frac{\Delta n\,(W_p)}{2\cosh\left(W_p/L_n\right)}\right]\cosh\left(x/L_n\right) \tag{9}$$

Next, we can get the electron current density as,

$$J_n = \frac{qD_n}{L_n}\tanh\left(\frac{W_p}{L_n}\right)\left[n_{po}\left(e^{\frac{V}{V_T}} - 1\right)\right] \tag{10}$$

Similarly, the hole concentration and its current density inside the n^+ emitter region in dark case could be written as owing to the boundary conditions (see Fig. 3(b)),

$$\Delta p\,(x) = A\,e^{-\frac{x}{L_p}} + Be^{\frac{x}{L_p}} \tag{11}$$

And

$$J_p = -\frac{qD_p}{L_p}\left[Ae^{\frac{-W_n}{L_p}} - Be^{\frac{W_n}{L_p}}\right] \tag{12}$$

where the constants A and B are found in the Appendix (Equations A.3 and A.4). Then, at dark condition, the overall current density is,

$$J_{dark} = 2 \times \left(J_n + J_p\right) \tag{13}$$

Then, the total current density of the vertical npn junctions is,

$$J_{Total} = J_{sc} + J_{dark} \tag{14}$$

Finally, the total npn structure performance is found by summing the total performance of the top planar structure (which is given by the conventional pn junction solar cell equations [14] and the total performance of vertical structure. The optical modeling and more details about the model are found in [16].

IV. N^+ EMITTER OPTIMIZATION

In this section, the n^+ emitter optimization is carried out for its sidewall surface treatment and its doping concentration.

A. EFFECT OF DIFFERENT N^+ EMITTER SIDEWALL SURFACE TREATMENTS

In this subsection, the influence of n^+ emitter sidewall surface treatment on the npn microstructure performance is investigated. This study is carried out for three different types of surface treatments which are: the ideal non-recombining contact surface with 0 cm/sec surface recombination velocity (v_s), the recombining contact with good oxidation for its surface, v_s equals 100 cm/sec, and ohmic contact with v_s equals 10^7cm/sec. The effect of such surface treatments on the structure performance is clarified using two ways. Firstly, the excess hole distribution inside the n^+ emitter region is demonstrated as it affects both the structure dark and illumination performance. Thus, it gives a perfect picture of the performance concerning the n^+ emitter sidewall surface treatments. The study of excess carriers' distribution is carried out at short circuit conditions, at which excess carriers are generated due to light. Secondly, a comparison between the structure electrical performance parameters for each case is presented. The simulation results of the three case studies are pictured in Fig. 4(a) which shows the excess holes distribution using our model inside n^+ emitter at three different values of v_s while Fig. 4(b) shows the variation of cell efficiency versus surface recombination velocity.

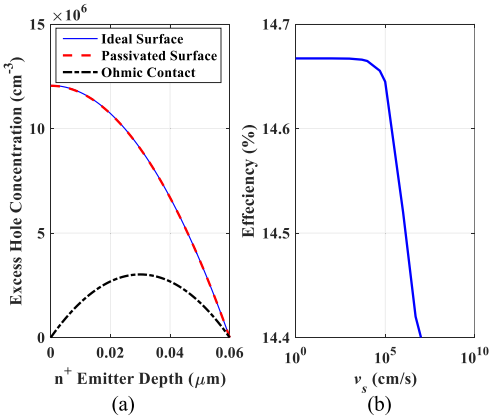

FIGURE 4. (a) Excess holes distribution inside the n^+ emitter for three different cases: Ideal non-recombining surface ($v_s = 0$), passivated recombining surface ($v_s = 100$ cm/s) and ohmic contact ($v_s = 10^7$ cm/sec). The excess holes are traced from 0 (the beginning of the sidewall emitter) through 0.06 μm (the end of the emitter thickness) (b) Variation of cell efficiency vs surface recombination velocity.

In the first case, the ideal non-recombining surface is studied. Such surfaces give the best performance as v_s equals zero, thus the excess holes distribution is maximum at sidewall surfaces. It means that there is no loss current due to surface recombination caused by n^+ emitter sidewall surfaces. Thus, the short circuit current enhances. In addition, the open circuit voltage is also enhanced as good passivation with zero or low v_s decreases the reverse saturation current by decreasing it gradient. Thus, it is important to treat the n^+ emitter sidewall surfaces on condition that v_s is very low to give best performance. It is important to study such an ideal surface as it gives the best performance, which is used as a reference for the other two cases. It can infer from Fig. 4 that the distribution of the excess holes is at its maximum value at the n^+ emitter sidewall and is zero at the junction boundary.

For the second case, the recombining surface, which is the practical surface treatment, is illustrated. To have a good n^+ emitter sidewall surface, it has to be passivated with good and clean oxide. Such oxide results in a low surface recombination velocity, v_s. As a result, both structure short circuit current and open circuit voltages are enhanced. Thus, to improve the npn solar cell performance, the sidewall surface of its n^+ emitter has to be treated with a low v_s recombining surface. This could be done by passivating the n^+ emitter sidewall surfaces using a clean oxide [29]–[32]. It has a low surface recombination velocity in the order of 100 cm/sec. As shown in Fig. 4(a), the excess holes distribution is reduced by a very little value at the n^+ emitter sidewall surface compared with the ideal case when v_s equals zero. This result emphasizes that the low v_s passivation performs close to the ideal non-recombining contact.

The third studied case of n^+ emitter sidewall surface is the ohmic contact assuming aluminum is deposited on n^+ emitter sidewall surface, the infinite recombining contact. The typical value for v_s for aluminum is between 10^7, 10^8cm/sec [33]–[35]. In this case, a great portion of the current component caused by the light generated carriers inside n^+ emitter region is lost due to sidewall high surface recombination. There is no excess holes distribution at the n^+ emitter sidewall surface as shown in Fig. 4(a). Thus, the short circuit current is decreased. Also, the open circuit voltage decreases slightly, as the infinite recombining contact increases the reverse saturation current.

A comparison of the electrical performance parameters of the npn structure at the three different studied cases of n^+ emitter sidewall surface treatment is addressed in Table 2. From the table, it is evident that the ohmic contact degrades the structure performance. It decreases J_{sc} because of the current loss component caused by surface recombination. Also, it decreases V_{oc} as it increases the reverse saturation current. For the conversion efficiency, it is reduced as expected. Based on the above discussion, it is recommended not to deposit aluminum on the n^+ emitter sidewall directly without passivating it first to get low values of v_s.

To get the maximum permissible surface recombination velocity at which the efficiency degradation is minor, we perform a simulation study to get the relation between the efficiency and v_s. In this regard, Fig. 4(b) shows the variation of the efficiency versus different values of surface

TABLE 2. Electrical performance parameters for the three different studied cases of n^+ emitter surface treatment.

v_s (cm/s)	0	100	10^7
J_{sc} (mA/cm^2)	40.23	40.22	39.71
V_{oc} (V)	0.583	0.583	0.582
FF (%)	82.32	82.32	82.34
η_c (%)	14.67	14.66	14.40

recombination velocity on the sidewalls. This study indicates that the surface recombination velocity should be kept below 10^4 cm/s because, as can be depicted from the figure, the efficiency drops when v_s is higher than 10^4 cm/s.

B. N^+ EMITTER DOPING CALIBRATION AND OPTIMIZATION

In this subsection, to optimize the n^+ emitter doping, firstly, the analytical model is calibrated using Silvaco TCAD [24] simulation for a case study of the npn solar cell microstructure [15]. The emitter doping calibration is carried out for 10^{18} cm^{-3} p^+ base doping and 8 μm base width (W_p). For the emitter width (W_n), it is taken to be 0.06 μm instead of the TCAD value of 0.1 μm [15]. The reason is that the npn microstructure analytical model is based on abrupt doping profiles [16], while, in Silvaco simulation, fabrication processes are taken into consideration using Athena process simulator.

Fig. 5 shows the calibration of the analytical model versus TCAD results of the n^+ emitter doping. It is clear that the results from the analytical model show a good agreement versus TCAD results. Moreover, the trend of the npn microstructure efficiency, for both results, with respect to the variation of the n^+ emitter doping level concentration is identical giving the most suitable choice at n^+ doping of $2 \times 10^{19} cm^{-3}$ [15].

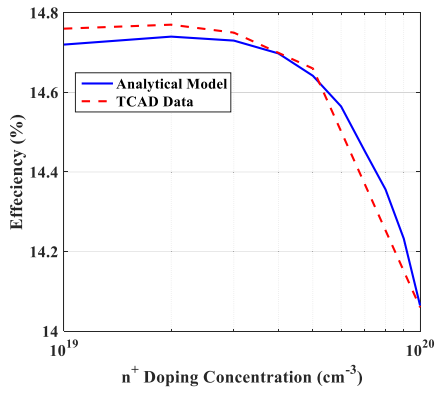

FIGURE 5. npn microstructure efficiency by analytical model vs SILVACO TCAD results: calibration of the n^+ emitter doping.

V. EFFECT OF BULK RECOMBINATION INSIDE P^+ BASE

In this section, the influence of bulk recombination inside the p^+ base on the npn solar cell microstructure performance is illustrated. Further, the efficiency resulted from the analytical model is also calibrated with TCAD results [15], at $10^{18} cm^{-3}$ p^+ base doping for different values of base width. The objective of this study is to show the impact of the bulk recombination, the relation between W_p and L_n, on the structure electrical performance.

The calibration is carried out to verify and determine the optimum W_p which gives the best efficiency at 10^{18} cm^{-3} p^+ base doping. Fig. 6 shows the efficiency versus W_p calculated analytically and by TCAD simulations. It is obvious that the maximum efficiency occurs at W_p equals 7 μm. The diffusion

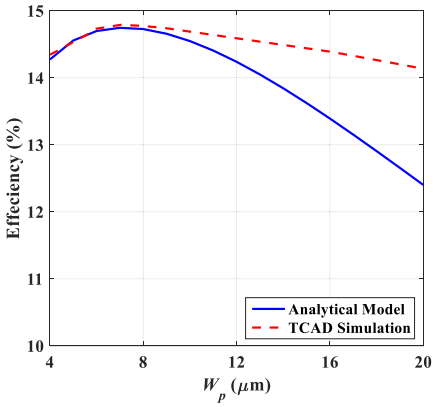

FIGURE 6. Calibration and optimization of efficiency versus W_p: analytical model results vs TCAD simulation at $10^{18} cm^{-3}$ p^+ base doping.

length, at the mentioned doping, is about 12 μm [26], so the $W_{p,optimum}/L_n$ ratio is near 0.6. Moreover, concerning the model results, the highest efficiency is 14.75% while it is 14.79% for TCAD simulation.

It should be pointed out here that using the analytical model is easier and gives a quick transparent solution in comparison with the time consuming TCAD device simulators irrespective to their high accuracy [16]. Thus, the behavior of the structure efficiency is easily predicted using its analytical model. The influence of W_p is obvious in the analytical model. So, the optimization of p^+ base doping and thickness is performed by the analytical model because it is more effective and time saving while maintains good accuracy versus TCAD simulations as discussed there before.

VI. THE EFFECT OF P^+ BASE DOPING VARIATION ON THE NPN MICROSTRUCTURE PERFORMANCE

In this section, the impact of the p^+ base doping concentration on the npn solar cell microstructure performance is illustrated. The main objective of this study is to figure out an appropriate way for achieving the highest efficiency of this low-cost silicon-based cell. The p^+ base width (W_p) is optimized for different values of the p^+ base doping level. Firstly, two values of the p^+ base doping concentration, 5×10^{17} cm^{-3} and 7×10^{17} cm^{-3}, less than the reference doping, $10^{18} cm^{-3}$, are investigated. Fig. 7(a) shows the cell efficiency versus W_p.

For $5 \times 10^{17} cm^{-3}$, the optimum W_p is 15 μm which gives the best efficiency of 15.89%. Concerning 7×10^{17} cm^{-3}, the optimum W_p is 10 μm at which the efficiency is 15.52%. These results are expected. When p^+ base doping decreases, L_n increases thus the optimum W_p also increases. As a result, the active area exposed to the input solar radiation spectrum increases. Accordingly, the illumination characteristics, J_{sc}, is enhanced. But it is important to mention that the structure cost increases with decreasing the p^+ base doping. Thus, regarding design criteria, one has to compromise between the required efficiency with respect to the structure cost.

Secondly, two values of the p^+ base doping concentration, 3×10^{18} cm^{-3} and 5×10^{18} cm^{-3}, higher than the reference

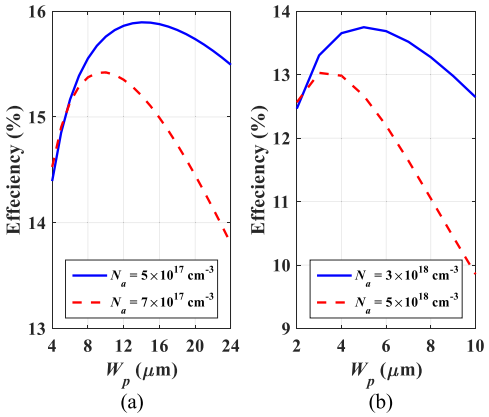

FIGURE 7. Cell efficiency vs W_p variation for (a) p^+ doping levels below 1×10^{18}cm^{-3} (5×10^{17} cm^{-3} and 7×10^{17}cm^{-3}) and (b) p^+ doping levels above 1×10^{18}cm^{-3} (3×10^{18} cm^{-3} and 5×10^{18} cm^{-3}).

doping, 10^{18}cm^{-3}, are investigated. Fig. 7(b) shows the npn structure efficiency versus W_p. For 3×10^{18} cm^{-3}, the optimum W_p is 5 μm at which the best efficiency is 13.75% while, for 5×10^{18}cm^{-3}, the optimum W_p is 3 μm giving a maximum efficiency of 13.03%.

Based on the above results, the npn microstructure efficiency at 5×10^{18}cm^{-3} is 13.03%. Such efficiency is considered high when compared to the low-cost solar cells, such as thin film solar cell. Thus, the npn structure performance is better than and dominating thin film solar cell [36]–[38], taking into consideration that the npn structure is not suffering from toxicity issues and practical usage limitations, like most of thin film solar cells. When comparing the npn solar cell microstructure with the c-Si based solar cells, its efficiency is lower than such cells. However, when comparing the npn structure with the c–Si based solar cell, one has to note that its doping is around 10^{18} cm^{-3} while the typical doping of the c-Si based solar cell is lower than 10^{17} cm^{-3}. It means that the npn structure does not need the costly process of zone refining like the case of the c–Si solar cell [39]–[41]. This is the reason for studying the effect of higher doping on the structure performance to achieve more reduction of its cost while conserving the acceptable efficiency and performance. Thus, two other higher p^+ base doping levels, 10^{19}cm^{-3} and 2×10^{19}cm^{-3} are studied. The doping of 2×10^{19} cm^{-3} is the near maximum doping of p^+ silicon rod out of the furnace before applying any zone refining process. Thus, the structure cost is greatly reduced for such p^+ base doping. Fig. 8 shows the cell efficiency versus W_p for 10^{19}cm^{-3} and 2×10^{19}cm^{-3} p^+ base doping.

Regarding the doping level of 10^{19} cm^{-3}, the maximum efficiency of 10.5% is obtained at an optimum W_p of 1.5 μm. Concerning 2×10^{19} cm^{-3}, the maximum efficiency of 9% is obtained at a lower value of optimum W_p which is 1 μm.

The npn microstructure efficiency which is 9% at 2×10^{19}cm^{-3} p^+ base doping is still accepted in comparison with thin film considering the expected ultralow cost of the structure because it requires no zone refining and no practical limitations. Thus, the npn solar cell microstructure achieves

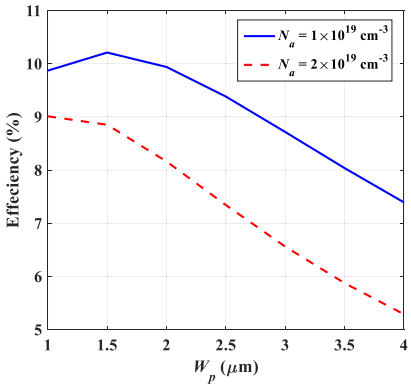

FIGURE 8. Cell efficiency versus W_p for very heavily doped base (1×10^{19} cm^{-3} and 2×10^{19} cm^{-3}).

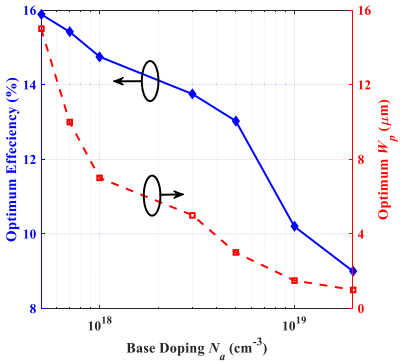

FIGURE 9. Optimum efficiency and base width for each value of p^+ base doping from 5×10^{17}cm^{-3} to 2×10^{19} cm^{-3}.

a competitive performance in higher doping levels. Besides, it has the advantages of no practical limitations such as toxicity and complicated fabrication processes.

Finally, Fig. 9 summarizes the npn structure optimum efficiency and base width for each value of p^+ base doping from 5×10^{17}cm^{-3} to 2×10^{19}cm^{-3}. The figure gives a clear picture about the relation between the p^+ base doping and the optimum width and efficiency. It is obvious that, both npn microstructure efficiency and W_p decreases with increasing p^+ base doping. The decline of the efficiency versus base doping is discussed therebefore. We emphasize here that as the base doping rises, the diffusion length decreases substantially. So, the base width, at which the maximum efficiency is attained, is decreased. Moreover, when the p^+ doping increases and, so, W_p decreases, the area exposed to the input solar radiation spectrum decreases, thus J_{sc} also decreases which results in decreasing the structure efficiency.

It should be mentioned here that increasing the doping concentration will approach the tunneling limit. This will be a research point in our future work.

VII. CONCLUSION

In this paper, by utilizing our previously published analytical model of the npn solar cell microstructure, we studied the impact of some crucial physical models on its performance. Also, some technological parameters of the cell were investigated to tackle their optimum values to get the highest

possible efficiency. The use of the analytical model gives a thorough physical insight about the behavior without the need for long TCAD simulation times or fabrication cost. Further, the calibrated analytical solution, provided in this work, is transparent, and the effect of the different parameters is easily and rapidly assessed. Also, the performance limits of the device were realized in a simple way and short times compared to the time consuming TCAD simulation. The main structure electrical performance parameters in all case studies were obtained to give a comparative inspection on the different cases.

Based on this analytical study, a good passivated n^+ emitter sidewall surface with low v_s below 10^4 cm/s is found to be necessary. It overcomes the microstructure performance degradation caused by surface recombination. A careful design of the base width of the structure is mandatory in order to overcome the bulk recombination which severely affects the performance of the npn microstructure. Based on the analytical simulation results, the structure base width has to be less than the electron diffusion length. For p^+ base doping concentration ranging from $5 \times 10^{17}\text{cm}^{-3}$ to $2 \times 10^{19}\text{cm}^{-3}$, the npn microstructure efficiency decreases from 15.9% to 9%, respectively.

These results emphasize that the npn solar cell microstructure still achieves a competitive efficiency at higher doping levels, for which its cost is significantly reduced, in comparison with thin film solar cell taking into consideration that the npn structure has the advantage of not suffering from the thin film solar cell practical limitations. Moreover, the use of higher doping levels permits lesser wafer area which is beneficial for large area solar cells design. Finally, the study sheds the light on the optimization of a cost-effective solar cell structure which is based on Silicon heavily doped wafers and brings some important design rules that should be fulfilled before working on fabrication processes.

APPENDIX

The physical parameters used in the analytical model equations are as follows:

q is the electron charge

μ_n, D_n are electron mobility and electron diffusion constant, respectively.

μ_p, D_p are hole mobility and hole diffusion constant, respectively.

E is the electric field

L_n is the electron diffusion length

The relation between L_n and D_n is $L_n^2 = D_n\tau_n$

L_p is the hole diffusion length

The relation between L_p and D_p is

$L_p^2 = D_p\tau_p$

For short circuit case, the constants A and B are given as,

$$A = \left[\frac{\left(-g_{ph}\,(y,\lambda)\,\tau_p\,e^{-W_n/L_p}\right)}{\left(D_p/v_sL_p - 1\right)}\right] \times \left[\frac{\left(D_p - v_sL_p\right)}{\left(\left(D_p - v_sL_p\right)e^{-W_n/L_p} + \left(D_p + v_sL_p\right)e^{W_n/L_p}\right)}\right] \tag{A.1}$$

$$B = \left[\left(\frac{D_p + v_sL_p}{D_p - v_sL_p}\right) + \left(\frac{-g_{ph}\,(y,\lambda)\,\tau_p}{D_p - v_sL_p}\right)\right] \times A \tag{A.2}$$

The constants A and B in dark case are given as,

$$A = \left[\frac{D_p - v_sL_p}{D_p + v_sL_p}\right] \times B \tag{A.3}$$

$$B = \left[\frac{\Delta p\,(W_n) \times \left(D_p + v_sL_p\right)}{\left(D_p + v_sL_p\right) \times e^{W_n/L_p} + \left(D_p - v_sL_p\right) \times e^{-W_n/L_p}}\right] \tag{A.4}$$

REFERENCES

[1] E. Scalise, "Tailoring the electronic properties of semiconducting nanocrystal-solids," *Semicond. Sci. Technol.*, vol. 35, no. 1, 2019, Art. no. 13001, doi: 10.1088/1361-6641/ab52e0.

[2] M. M. Salah, K. M. Hassan, M. Abouelatta, and A. Shaker, "A comparative study of different ETMs in perovskite solar cell with inorganic copper iodide as HTM," *Optik*, vol. 178, pp. 958–963, Feb. 2019, doi: 10.1016/j.ijleo.2018.10.052.

[3] O. A. M. Abdelraouf, A. Shaker, and N. K. Allam, "Novel design of plasmonic and dielectric antireflection coatings to enhance the efficiency of perovskite solar cells," *Sol. Energy*, vol. 174, pp. 803–814, Nov. 2018, doi: 10.1016/j.solener.2018.09.066.

[4] Z. Shi, X. Wang, Y. Sun, Y. Li, and L. Zhang, "Interlayer coupling in two-dimensional semiconductor materials," *Semicond. Sci. Technol.*, vol. 33, no. 9, Sep. 2018, Art. no. 093001, doi: 10.1088/1361-6641/aad6c3.

[5] A. Ebong, M. Hilali, V. Upadhyaya, S. Rounsaville, I. Ebong, and A. Rohatgi, "High efficiency screen-printed planar solar cells on single crystalline silicon materials," in *Proc. Conf. Rec. 31st IEEE Photovoltaic Spec. Conf.*, Jan. 2005, pp. 1173–1176, doi: 10.1109/PVSC.2005.1488347.

[6] S. Peters, C. Ballif, D. Borchert, R. Schindler, W. Warta, and G. Willeke, "Record fast thermal processing of 17.5 efficient silicon solar cells," *Semicond. Sci. Technol.*, vol. 17, no. 7, pp. 677–681, Jul. 2002, doi: 10.1088/0268-1242/17/7/307.

[7] I. Hamammu and K. Ibrahim, "Low cost fabrication for high efficiency monocrystalline silicon solar cells," in *Proc. 3rd World Conf. Photovoltaic Energy Convers.*, vol. 2, May 2003, pp. 1519–1520.

[8] K. Murukesan and N. R. Mavilla, "Towards fabrication of low cost high efficiency c-Si solar cells: Progress and optimization using TCAD simulation study," in *Proc. 38th IEEE Photovoltaic Spec. Conf.*, Jun. 2012, pp. 2218–2222, doi: 10.1109/PVSC.2012.6318037.

[9] L. J. Geerligs, I. G. Romijn, A. R. Burgers, N. Guillevin, A. W. Weeber, J. H. Bultman, H. Wang, F. Lang, W. Zhao, G. Li, Z. Hu, J. Xiong, and A. Vlooswijk, "Progress in low-cost n-type silicon solar cell technology," in *Proc. 38th IEEE Photovoltaic Spec. Conf.*, Jun. 2012, pp. 1701–1704, doi: 10.1109/PVSC.2012.6317923.

[10] B. M. Kayes, H. A. Atwater, and N. S. Lewis, "Comparison of the device physics principles of planar and radial p-n junction nanorod solar cells," *J. Appl. Phys.*, vol. 97, no. 11, Jun. 2005, Art. no. 114302, doi: 10.1063/1.1901835.

[11] E. C. Garnett and P. Yang, "Silicon nanowire radial p-n junction solar cells," *J. Amer. Chem. Soc.*, vol. 130, no. 29, pp. 9224–9225, Jul. 2008, doi: 10.1021/ja8032907.

[12] M. S. Salem, A. Shaker, M. Abouelatta, and A. Zekry, "Effect of base width variation on the performance of a proposed ultraviolet low cost high efficiency solar cell structure," in *Proc. 38th IEEE Photovoltaic Spec. Conf.*, Jun. 2012, Art. no. 000775, doi: 10.1109/PVSC.2012.6317718.

[13] M. S. Salem, A. Zekry, A. Shaker, and M. Abouelatta, "Design and simulation of proposed low cost solar cell structures based on heavily doped silicon wafers," in *Proc. IEEE 43rd Photovoltaic Spec. Conf. (PVSC)*, Jun. 2016, pp. 2393–2397.

[14] A. Zekry, A. Shaker, and M. Salem, "Solar cells and arrays: Principles, analysis, and design," in *Advances in Renewable Energies and Power Technologies*. Amsterdam, The Netherlands: Elsevier, vol. 1, 2018, pp. 3–56.

[15] M. S. Salem, A. Zekry, A. Shaker, M. Abouelatta, and T. M. Abdolkader, "Performance enhancement of a proposed solar cell microstructure based on heavily doped silicon wafers," *Semicond. Sci. Technol.*, vol. 34, no. 3, Mar. 2019, Art. no. 035012.
[16] M. S. Salem, A. J. Alzahrani, R. A. Ramadan, A. Alanazi, A. Shaker, M. Abouelatta, C. Gontrand, M. Elbanna, and A. Zekry, "Physically based analytical model of heavily doped silicon wafers based proposed solar cell microstructure," *IEEE Access*, vol. 8, pp. 138898–138906, 2020, doi: 10.1109/ACCESS.2020.3012657.
[17] M. D. Kelzenberg, D. B. Turner-Evans, B. M. Kayes, M. A. Filler, M. C. Putnam, N. S. Lewis, and H. A. Atwater, "Single-nanowire Si solar cells," in *Proc. 33rd IEEE Photovolatic Spec. Conf.*, May 2008, pp. 1–6, doi: 10.1109/PVSC.2008.4922736.
[18] M. C. Putnam, S. W. Boettcher, M. D. Kelzenberg, D. B. Turner-Evans, J. M. Spurgeon, E. L. Warren, R. M. Briggs, N. S. Lewis, and H. A. Atwater, "Si microwire-array solar cells," *Energy Environ. Sci.*, vol. 3, no. 8, pp. 1037–1041, 2010, doi: 10.1039/C0EE00014K.
[19] H. Bashiri, M. A. Karami, and S. M. Nejad, "An analytical approach for modeling of high-efficiency crystalline silicon solar cells with homo–hetero junctions," *Mater. Sci. Semicond. Process.*, vol. 111, Jun. 2020, Art. no. 104960, doi: 10.1016/j.mssp.2020.104960.
[20] N. M. Ali, N. K. Allam, A. M. Abdel Haleem, and N. H. Rafat, "Analytical modeling of the radial pn junction nanowire solar cells," *J. Appl. Phys.*, vol. 116, no. 2, Art. no. 24308, Jul. 2014, doi: 10.1063/1.4886596.
[21] H. D. Um, K. Lee, I. Hwang, J. Park, D. Choi, N. Kim, H. Kim, and K. Seo, "Progress in silicon microwire solar cells," *J. Mater. Chem. A*, vol. 8, no. 11, pp. 5395–5420, 2020.
[22] A. Zekry, "A road map for transformation from conventional to photovoltaic energy generation and its challenges," *J. King Saud Univ. Eng. Sci.*, vol. 32, no. 7, pp. 407–410, Nov. 2020.
[23] K. Peng, A. Lu, R. Zhang, and S.-T. Lee, "Motility of metal nanoparticles in silicon and induced anisotropic silicon etching," *Adv. Funct. Mater.*, vol. 18, no. 19, pp. 3026–3035, Oct. 2008.
[24] T. C. Yang, B. S. Lee, and T. J. Yen, "Minimizing reflection losses from metallic electrodes and enhancing photovoltaic performance using the Si-micrograting solar cell with vertical sidewall electrodes," *Appl. Phys. Lett.*, vol. 101, no. 10, 2012, Art. no. 103902.
[25] J. A. del Alamo and R. M. Swanson, "Modelling of minority-carrier transport in heavily doped silicon emitters," *Solid-State Electron.*, vol. 30, no. 11, pp. 1127–1136, Nov. 1987.
[26] A. Zekry, "The dependence of diffusion length, lifetime and emitter gummel-number on temperature and doping," *Archiv Fur Elektrotechnik*, vol. 75, no. 2, pp. 147–154, Mar. 1992.
[27] A. Zekry, A. Shaker, M. Ossaimee, M. S. Salem, and M. Abouelatta, "A comprehensive semi-analytical model of the polysilicon emitter contact in bipolar transistors," *J. Comput. Electron.*, vol. 17, no. 1, pp. 246–255, Mar. 2018.
[28] *Athena and Atlas User's Manual Process and Device Simulation Software*, Silvaco International, Santa Clara, CA, USA, 2016.
[29] N. E. Grant and K. R. McIntosh, "Low surface recombination velocity on (100) silicon by electrochemically grown silicon dioxide annealed at low temperature," *IEEE Electron Device Lett.*, vol. 31, no. 9, pp. 1002–1004, Sep. 2010.
[30] H. Jin and K. J. Weber, "Relationship between interface defect density and surface recombination velocity in (111) and (100) silicon /silicon oxide structure," in *Proc. 23rd Eur. Photovoltaic Solar Energy Conf.*, Sep. 2008, pp. 1–5.
[31] S. Gatz, J. Müller, T. Dullweber, and R. Brendel, "Analysis and optimization of the bulk and rear recombination of screen-printed PERC solar cells," *Energy Procedia*, vol. 27, pp. 95–102, Jan. 2012.
[32] M. Dremel and P. Würfel, "Surface recombination at the Si-SiO_2 interface," *Proc. 10th Workshop Quantum Sol. Energy Convers. (QUANTSOL)*, Bad Hofgastein, Austria, Mar. 1998. [Online]. Available: http://www.quantsol.org/pub/pub_6.htm
[33] P. Lolgen, J. A. Leguijt, R. A. Eikelboom, R. A. Steeman, W. C. Sinke, L. A. Verhoef, P. F. A. Alkemade, and E. Algra., "Aluminum back-surface field doping profiles with surface recombination velocities below 200 cm/s," in *Proc. Photovoltaic Spec. Conf.*, May 1993, pp. 236–242.
[34] S. Narasimha, A. Rohatgi, and A. W. Weeber, "An optimized rapid aluminum back surface field technique for silicon solar cells," *IEEE Trans. Electron Devices*, vol. 46, no. 7, pp. 1363–1370, Jul. 1999.
[35] S. Gatz, K. Bothe, J. Müller, T. Dullweber, and R. Brendel, "Analysis of local al-doped back surface fields for high efficiency screen-printed solar cells," *Energy Procedia*, vol. 8, pp. 318–323, Jan. 2011.
[36] A. Lambertz, F. Finger, R. E. I. Schropp, U. Rau, and V. Smirnov, "Preparation and measurement of highly efficient a-Si:H single junction solar cells and the advantages of μc-siOx:Hn-layers," *Prog. Photovoltaics: Res. Appl.*, vol. 23, no. 8, pp. 939–948, Aug. 2015, doi: 10.1002/pip.2629.
[37] H. Sai, K. Maejima, T. Matsui, T. Koida, M. Kondo, S. Nakao, Y. Takeuchi, H. Katayama, and I. Yoshida, "High-efficiency microcrystalline silicon solar cells on honeycomb textured substrates grown with high-rate VHF plasma-enhanced chemical vapor deposition," *Jpn. J. Appl. Phys.*, vol. 54, no. 8S1, 2015, pp. Art. no. 08KB05, doi: 10.7567/JJAP.54.08KB05.
[38] H. Sai, T. Matsui, H. Kumagai, and K. Matsubara, "Thin-film microcrystalline silicon solar cells: 11.9% efficiency and beyond," *Appl. Phys. Exp.*, vol. 11, no. 2, Feb. 2018, Art. no. 022301, doi: 10.7567/APEX.11.022301.
[39] J. Liu, Y. Yao, S. Xiao, and X. Gu, "Review of status developments of high-efficiency crystalline silicon solar cells," *J. Phys. D, Appl. Phys.*, vol. 51, no. 12, Mar. 2018, Art. no. 123001, doi: 10.1088/1361-6463/aaac6d.
[40] J.-T. Lin, C.-C. Lai, C.-T. Lee, Y.-Y. Hu, K.-Y. Ho, and S. W. Haga, "A high-efficiency HIT solar cell with pillar texturing," *IEEE J. Photovolt.*, vol. 8, no. 3, pp. 669–675, May 2018, doi: 10.1109/JPHOTOV.2018.2804330.
[41] K. Yoshikawa, W. Yoshida, T. Irie, H. Kawasaki, K. Konishi, H. Ishibashi, T. Asatani, D. Adachi, M. Kanematsu, H. Uzu, and K. Yamamoto, "Exceeding conversion efficiency of 26% by heterojunction interdigitated back contact solar cell with thin film Si technology," *Sol. Energy Mater. Sol. Cells*, vol. 173, pp. 37–42, Dec. 2017.

MARWA S. S. BASYONI was born in Gedda, Saudi Arabia, in 1979. She received the B.Sc. degree from the Electronics and Communications Engineering Department, Faculty of Engineering, Ain Shams University, Cairo, Egypt, in 2002, and the master's degree in renewable energy and the Ph.D. degree in renewable energy, especially in solar cells, from Ain Shams University, in 2006 and 2013, respectively. From 2003 to 2013, she worked as a Research Assistant with the Faculty of Engineering, Ain Shams University. She is currently the Vice Dean of the Computer College, University of Ha'il, Ha'il, Saudi Arabia. Her research interests include VLSI design, MEMS technology, nano technology, renewable energy, solar cell, PV systems, semiconductor physics, simulation, and modeling of power devices.

A. ZEKRY (Member, IEEE) graduated from Cairo University, Egypt, in 1969. He received the M.Sc. degree from Cairo University, in 1973, and the Ph.D. degree from TU Berlin, in 1981. He worked as a Scientific Coworker with TU Berlin. He was a staff member on several rewarded universities. He is currently a Professor of electronics with the Faculty of Engineering, Ain Shams University, Cairo, Egypt. He has supervised over 100 master thesis and 30 Ph.D. dissertations. He has also authored and coauthored over 240 conference and periodical papers. His current research interests include microelectronics and electronic applications, including communications and photovoltaics. He received several prizes for the acknowledgment of his outstanding research and teaching performance.

AHMED SHAKER was born in Cairo, Egypt. He received the M.Sc. and Ph.D. degrees from Ain Shams University, Cairo, in 2003 and 2010, respectively.

Since 1997, he has been with the Engineering Physics Department, Faculty of Engineering, Ain Shams University, where he is currently an Associate Professor. Recently, he joined the Electrical and Computer Engineering (ECE) Department, North Carolina State University (NCSU), Raleigh, USA, as a Postdoctoral Researcher, where he is involved in solar cell and GaN-based LEDs fabrication and modeling. His research interests include simulation and modeling of semiconductor power devices, solar cells, 3D detectors, and nanoscale devices, including TFETs and CNTFETs.